View metadata, citation and similar papers at core.ac.uk

brought to you by CORE

provided by Institutionelles Repositorium der Leibniz Universität Hannover

PHYSICAL REVIEW B **77**, 024311 (2008)

Li jump process in h-$Li_{0.7}TiS_2$ studied by two-time ^{7}Li spin-alignment echo NMR and comparison with results on two-dimensional diffusion from nuclear magnetic relaxation

M. Wilkening* and P. Heitjans†

Institute of Physical Chemistry, and Center for Solid State Chemistry and New Materials, Leibniz University Hannover, Callinstraße 3A, D-30167 Hannover, Germany

(Received 25 May 2007; revised manuscript received 23 November 2007; published 31 January 2008)

^{7}Li spin-alignment NMR is used to trace ultraslow diffusion of Li^+ in the layered Li conductor Li_xTiS_2 ($x=0.7$). Two-time correlation functions were recorded for fixed evolution times as a function of mixing time at temperatures within the ^{7}Li rigid-lattice regime. The corresponding decay rates were identified as Li jump rates τ^{-1} ranging from 10^{-1} to 10^3 s^{-1} between temperatures $T=148$ K and 213 K. The jump rates obtained directly from spin-alignment echo NMR and those from diffusion induced maxima of spin-lattice relaxation peaks, monitored in the laboratory as well as in the rotating frame, are consistent with each other and follow an Arrhenius law with an activation energy of 0.41(1) eV and a preexponential factor of $6.3(1)\times10^{12}$ s^{-1}. Altogether, a solitary Li diffusion process was found between 148 and 510 K. Li diffusion was investigated in a dynamic range of about 10 orders of magnitude, i.e., $0.1\leqslant\tau^{-1}\leqslant7.8\times10^8$ s^{-1}. Additionally, the analysis of final-state echo amplitudes of the two-time correlation functions revealed information about the Li diffusion pathway in $Li_{0.7}TiS_2$. Obviously, a two-site jump process is present, i.e., besides the regularly occupied octahedral sites also the vacant tetrahedral ones within the van der Waals gap are involved in the overall two-dimensional diffusion process.

DOI: 10.1103/PhysRevB.77.024311 PACS number(s): 66.30.−h, 76.60.−k, 76.60.Lz, 82.47.Aa

I. INTRODUCTION

Nuclear magnetic resonance (NMR) is a well-known powerful tool for the investigation of structure and dynamics in condensed matter. Especially, it is highly suitable to study cation dynamics in fast Li ion conducting materials which are required for the design of new secondary Li batteries in everyday use.[1–7] Moreover, in recent years many studies have focused attention on lithium conductors because of their potential application in electrochromic displays[8] as well as in chemical sensors, see, e.g., Refs. 9 and 10.

Layered lithium titanium disulfide, Li_xTiS_2, is one of the first materials which were used as an electrode material in a rechargeable Li ion battery.[11,12] For this reason, it is one of the best investigated intercalation compounds at all.[13,14] Although Li diffusion in Li_xTiS_2 was studied in previous years by others using ^{7}Li NMR relaxation experiments,[15–19] a comprehensive study about the cation dynamics, especially in the regime of ultraslow Li motions which are not accessible by standard measurements, is still missing. Unfortunately, the standard tracer technique is not applicable to study Li dynamics due to the lack of a suitable radioactive Li isotope. Therefore, it is a necessity in general that ^{7}Li NMR methods are steadily developed to overcome this disadvantage. It is the aim of the present paper to show that newly developed[20,21] but not yet well-established ^{7}Li spin-alignment echo (SAE) NMR, i.e., the recording of Jeener-Broekaert echoes[22] of spin-3/2 nuclei, can be used to probe directly Li jump rates with values in the kilohertz to subhertz regime. Such extremely slow Li motions are not or only hardly accessible by other NMR methods. *Directly* means here that no theoretical model was necessary to convert the measured echo decay rates into microscopic Li jump rates. By applying the SAE technique, it is possible to enlarge the experimental time window for studying ^{7}Li jumps because the well-known ^{7}Li relaxation NMR methods probe Li jump rates on much shorter time scales.[23]

Here, we report on the measurement of ultraslow translational ^{7}Li jumps on the millisecond to second time scale by static stimulated-echo NMR spectroscopy in polycrystalline hexagonal $Li_{0.7}TiS_2$ at temperatures where no significant motional narrowing of the NMR linewidth has set in. The results are compared with those from various relaxation NMR experiments[23] probing much faster Li jump rates. Under certain conditions, also relaxation NMR allows the model-independent determination of jump rates, however, at much higher temperatures and in a more restricted way than it is possible via SAE NMR. The combination of different ^{7}Li NMR techniques allowed the direct measurement of a solitary Li diffusion process in $Li_{0.7}TiS_2$ over a dynamic range of about 10 decades. $Li_{0.7}TiS_2$ served as a model substance for this comprehensive and unprecedented investigation of two-dimensional Li diffusion by ^{7}Li two-time SAE NMR spectroscopy. ^{7}Li NMR relaxation data will be analyzed with respect to the two-dimensional (2D) nature of Li diffusion in Li_xTiS_2. Furthermore, first measurements of the alignment-echo final states containing information about the diffusion pathway[21,24–26] in h-$Li_{0.7}TiS_2$ are discussed. The present paper details and greatly extends a preliminary letter version.[27]

II. LITHIUM TITANIUM DISULFIDE

TiS_2 exists in two modifications, a layered and a cubic one.[28,29] The hexagonal (h) as well as the cubic polymorph are known as fast lithium ion conductors.[30,31] However, at room temperature, Li diffusion in the layered modification is about ten times faster than in the cubic one.[31–33] Li ions can be easily inserted into the van der Waals gap of the layered host TiS_2 (CdI_2-type structure, space group $P\bar{3}m1$) electro-

 ©2008 The American Physical Society

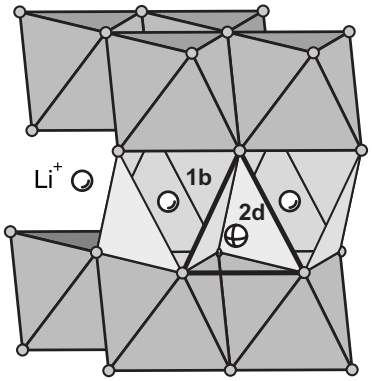

FIG. 1. Structure of h-$Li_{0.7}TiS_2$ ($P\bar{3}m1$). Small gray circles show the positions of S anions coordinating Ti cations octahedrally. Between the TiS_2 layers, small Li cations (white circles) can be intercalated. Li cations preferentially occupy octahedral sites (1b). The tetrahedral site (2d), highlighted by bold lines, may be a transition structure during the Li hopping process between two octahedral positions. An Li cation temporarily visiting the tetrahedral site is marked with a cross.

chemically as well as chemically by treatment with, e.g., n-butyl lithium. The topotactical intercalation process is fully reversible.[3] h-Li_xTiS_2 is a first stage intercalation compound.[3,34] It is stable over the whole intercalation range ($0<x\leqslant 1$) and shows only a single phase.[3] Its thermal stability as well as its simple layered structure make it a singularly well-defined material for the study of cation diffusion confined to two dimensions. The low dimensionality of the Li diffusion process was unambiguously shown for the compound with $x=0.7$ by ^{7}Li solid state NMR spin-lattice relaxation rate measurements.[30] h-Li_xTiS_2 is one of only few examples where the 2D nature of cation diffusion was probed by frequency and temperature dependent measurements, see, e.g., Ref. 35 for an analogous ^{1}H NMR relaxation study of proton diffusion in polycrystalline $ZrBe_2H_{1.4}$. Li^+ ions in h-Li_xTiS_2 reside preferentially in octahedral sites between the TiS_2 layers[36] (see Fig. 1). In compositions with $x<1$, the cations are highly mobile[15,30] due to vacant octahedral sites ($1b$) within the van der Waals gap. It has been suggested that the tetrahedral site (2d) is involved in the Li diffusion process as a transition structure for Li^+ hopping between two $1b$ positions.[37] The same diffusion pathway was recently postulated for isostructured Li_xTiSe_2 (see Refs. 38–40).

III. ACCESSIBLE TIME SCALES BY NMR

With classical NMR relaxation methods, different time scales of local ionic motions are accessible (Fig. 2). Experimentally, the easiest way to get access to microscopic Li diffusion parameters like jump rates and energy barriers is the measurement of the diffusion induced ^{7}Li NMR spin-lattice relaxation rate $T_{1\mathrm{diff}}^{-1}$ (see Ref. 23). $T_{1\mathrm{diff}}^{-1}$ as a function of inverse temperature $1/T$ will go through a maximum at $\omega_0\approx 1/\tau$, identifying $1/\tau$ as the jump rate of the hopping ion. $T_{1\mathrm{diff}}^{-1}$ will vary rapidly on either side of this maximum. The low-T flank of the peak might be affected by correlation

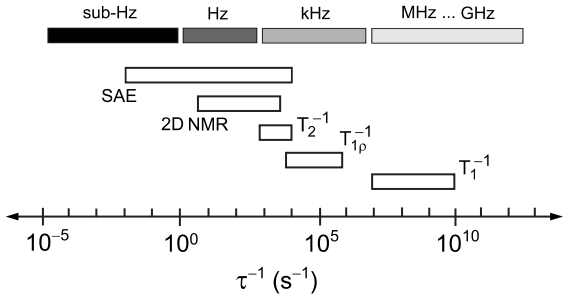

FIG. 2. ^{7}Li NMR techniques and corresponding timescales on which cation dynamics can be probed. See Sec. III for the explanation of the abbreviations used.

effects,[41,42] leading to a decrease of the corresponding slope. The high-T slope is influenced only when the dimensionality of the diffusion process is lower than 3.[23] Whereas $T_{1\mathrm{diff}}^{-1}$ is sensitive to diffusive motion with jump rates in the region of the frequency $\omega_0/2\pi$, which in practice may be varied from about 10 MHz to several hundred megahertz, slower ionic motions can be probed by recording diffusion induced spin-lattice relaxation rates $T_{1\rho\mathrm{diff}}^{-1}$ in the rotating frame.[23,43–45] $T_{1\rho\mathrm{diff}}^{-1}$ vs $1/T$ shows a maximum at $\omega_1\approx 1/\tau$, i.e., at lower temperature, because $\omega_1/2\pi$, which is the locking frequency, is much smaller than $\omega_0/2\pi$ and lies typically in the kilohertz range. While there have been several papers reporting jump rates over a large dynamic range (see, e.g., Refs. 44, 46, and 47), these have been evaluated using various models for the shapes of the relaxation peaks. However, in the present case, the jump rates were determined independently of a specific model, i.e., solely from the frequency dependent positions (on the temperature scale) of the maxima of the corresponding relaxation rate peaks. In addition to T_1^{-1} and $T_{1\rho}^{-1}$ measurements, also solid echo NMR spectroscopy, i.e., the analysis of changes of ^{7}Li NMR line shapes or the measurement of the ^{7}Li NMR spin-spin relaxation rate T_2^{-1}, reveals information about ionic motions in the kilohertz range depending on the modulation of interactions between the nucleus and the surrounding magnetic and/or electric fields through the dynamic process. In the case of ^{7}Li, jump rates between 10^4 and 10^3 s^{-1} are usually accessible.

Ionic motions on the ultraslow time scale, i.e., in the hertz to subhertz range, are hardly accessible by recording line shapes or spin-spin relaxation times because such extremely slow motions with jump rates smaller than 10^3 s^{-1} have no or only a marginal effect on the line shape. Up to now, only few multidimensional NMR experiments have been applied on solid ion conductors to enlighten very slow motions of ^{6}Li and ^{7}Li ions, respectively. For the first time, 2D exchange NMR [rotor synchronized magic angle spinning (MAS) NMR] was carried out by Xu and Stebbins[48] to observe ^{6}Li hopping dynamics among multiple crystallographic sites in polycrystalline Li_4SiO_4. Recently, details of Li diffusivity in $LiMn_2O_4$ were probed directly by 2D ^{7}Li MAS NMR by Verhoeven *et al.*[49] This work was followed by 2D NMR investigations on Li_7MnN_4 by Cabana *et al.*[50] as well as on monoclinic $Li_3V_2(PO_4)_3$ by Cahill *et al.*[51] Quite recently, van Wüllen *et al.* used cross-polarized ^{6}Li-{^{7}Li} MAS-NMR to

study Li dynamics in the hexaoxometalate Li_7TaO_6 (Ref. 52) as well as in the garnet $Li_5La_3Nb_2O_{12}$.[53]

In addition or alternatively to exchange NMR, the measurement of multiple-time correlation functions can be used to investigate directly ultraslow translational as well as rotational motions. SAE NMR spectroscopy of deuterons ^2H with spin quantum number $I=1$ was originally developed by Spiess and coworkers.[54,55] The method proved to be a successful tool for the study of deuteron dynamics. Furthermore, it provides detailed information about the type of molecular motion.[24–26] Quite recently, static SAE NMR spectroscopy was also applied to quadrupole nuclei with a spin-quantum number I of 3/2. First, Tang *et al.*[20,56,57] recorded ^9Be NMR spin-alignment echoes to study ultraslow ionic motions in a metallic beryllium containing glass in order to reveal the prevailing diffusion mechanism in this material. The method was then used by Böhmer and co-workers[58,59] to investigate ultraslow Li motions in crystalline $Li_3Sc_2(PO_4)_3$ and $Li_3In_2(PO_4)_3$. In that work, ultraslow motions of the ^7Li nucleus were studied by recording two-time translational correlation functions for the first time. Moreover, spin-alignment NMR spectroscopy was used to characterize lithium diffusion in a number of dielectric materials such as β-eucryptite,[60,61] the glass ceramic Zerodur M (Schott),[62] as well as in glassy and crystalline β-spodumene.[61,63] Besides an early account on hexagonal $Li_{1.0}TiS_2$,[64] we also reported on first SAE NMR measurements on cubic $Li_{0.6}TiS_2$.[31] Furthermore, we have used the ^7Li spin-alignment technique to study extremely slow Li dynamics in a series of single crystalline, polycrystalline, as well as amorphous Li conductors such as Li_3N,[32,65] Li_4SiO_4,[66] $Li_4Ti_5O_{12}$,[67] and $LiNbO_3$.[68]

It is worth mentioning in this context that ^{109}Ag stimulated echo NMR two- and four-time correlation functions were recorded recently to investigate silver dynamics in glasses of the compositions $(AgI)_x$-$(AgPO_3)_{(1-x)}$,[69–72] $(AgI)_x$-$(Ag_2O$-$B_2O_3)_{(1-x)}$,[73] as well as in several other Ag compounds.[74,75] In contrast to spin-1 and spin-3/2 nuclei, in the case of the nonquadrupolar ^{109}Ag nucleus with $I=1/2$ chemical shift interactions are used to differentiate between the ions.

IV. SPIN-ALIGNMENT ECHO NMR

The principle idea of spin-alignment echo NMR spectroscopy is similar to that of 2D exchange NMR. Whereas by means of the latter one chemical shift interactions are considered, SAE NMR takes advantage of interactions between the quadrupole moment of the nucleus and the electric field gradient (EFG) tensor at its site. In exchange NMR, magnetization is produced that is labeled by chemical shift interactions due to magnetically nonequivalent crystallographic sites where the nuclei reside. The magnetization is stored so that exchange can occur before it is sampled. If there is exchange, i.e., if hopping of the ions between magnetically distinct sites occurs, the magnetization is now labeled with a different shift frequency and shows up as crosspeak, i.e., off-diagonal intensity, in a 2D plot. The quadrupole interaction, which is used in ^7Li SAE NMR instead of chemical shift interactions in usual exchange NMR, is described by the Hamiltonian[76]

$$\hat{H}_q = \frac{1}{4}\frac{e^2qQ}{2I(2I-1)}(3\hat{I}_z - \hat{I}^2)(3\cos^2\Theta - 1 - \eta_q \sin^2\Theta\cos 2\Phi). \quad (1)$$

Here, e and eq are the proton charge and the principle component of the electric field gradient tensor, respectively. Q is the electric quadrupole moment of the nucleus. The angles θ and ϕ specify the orientation of the external field B_0 in the principle axis system of the EFG tensor at the nucleus site. $\hat{I}$ and $\hat{I}_z$ are the nuclear spin operators and γ is the magnetogyric ratio of the respective nucleus. η_q is the asymmetry parameter of the quadrupole interaction.

The quadrupole interaction alters the Zeeman frequency ω_0 toward $\omega_0 \pm \omega_Q$. The corresponding quadrupole frequency is given by

$$\omega_Q = \pm \delta\pi/2[3\cos^2\Theta - 1 - \eta\sin^2\Theta\cos(2\Phi)], \quad (2)$$

with the quadrupole coupling constant $\delta = e^2qQ/h$, where h is Planck's constant.

Provided electrically inequivalent sites are visited on a given diffusion pathway by the jumping ion, the information about the dynamic process is coded in terms of a change in the angular quadrupole frequency ω_Q. The spin-alignment technique allows the measurement of a single-particle correlation function yielding information about dynamic as well as geometric parameters of the hopping process.

The pulse sequence used to sample alignment echoes is based on the Jeener-Broekaert (JB) experiment,[22]

$$(90°)_x - t_p - (45°)_y - t_m - (45°)_\phi - t - \text{aquisition}.$$

The phase ϕ of the third pulse is arbitrary. In the ideal case, the first two pulses generate longitudinal pure quadrupole spin order. To avoid as much as possible the preparation of, e.g., dipolar simultaneously with quadrupolar order, proper pulse phasing is necessary and in the case of ^7Li the preparation time usually has to be chosen short; values smaller than 20 μs are typical. However, this choice depends on the strength of the specific interactions. Here, sin-sin two-time correlation functions were recorded for various preparation times t_p ranging from 5 to 150 μs. The third or reading pulse of the JB-sequence transforms spin alignment back into an observable transverse coherent magnetization leading to an echo at $t=t_p$. The amplitude of the spin-alignment echo is given by[21]

$$S_2(t_p,t_m) = \tfrac{9}{20}\langle \sin[\omega_Q(t_m=0)t_p]\sin[\omega_Q(t_m)t_p]\rangle. \quad (3)$$

Here, $\langle\cdots\rangle$ denotes the powder average. The decay of stimulated echo amplitudes $S_2(t_p,t_m)$ for fixed t_p and as a function of t_m is in general due to two processes, i.e., (i) individual jumps of the ions and (ii) spin-lattice relaxation. The first one will affect the echo formation when the ions jump between sites with different quadrupole frequencies. Thus, as mentioned above, in a stimulated-echo experiment, the frequency change from the initial value $\omega_Q(t_m=0)$ to the final one $\omega_Q(t_m)$, experienced by the jumping ion, opens a way for a

direct measurement of the correlation time τ. Simultaneously, the second process gives rise to a decay of quadrupolar order and, thus, to an additional decrease of the alignment echo amplitude. This means that the experimental time window to investigate ionic motions is limited by spin-lattice relaxation and one has to choose t_m to be smaller than T_1. The evolution time t_p, however, refers to intervals of precessing magnetization and is limited to be less than the spin-spin-relaxation time T_2, which is about 100 μs for h-$Li_{0.7}TiS_2$ in the rigid lattice regime ($T<240$ K). In h-$Li_{0.7}TiS_2$, the spin-lattice relaxation time T_1 is of the order of several seconds below room temperature. Hopping correlation times, however, are expected to be of the order of seconds to milliseconds in this temperature range. Thus, it should be possible to distinguish between the two processes easily. In fact, the measured decay curves reveal two separable regimes, one which is due to ionic motion and a second one arising from non-diffusive spin-lattice relaxation effects.

Especially in the case of ^{7}Li being subject to relatively strong homonuclear dipole-dipole interactions as compared to, e.g., ^{9}Be, the complete suppression of dipolar (D) order showing up simultaneously with quadrupolar (Q) order is difficult to realize.[59,60,63,66] This is because the two corresponding time constants $\tau_{SAE,D}$ and $\tau_{SAE,Q}$ determining the echo decay will be of the same order of magnitude. The decay of dipolar order, if present, will be slightly faster than the single-particle process. Whereas pure spin-alignment NMR leads directly to a single-particle correlation function, the decay of dipolar order is described by at least a two-particle correlation function. The impact of homonuclear dipolar interactions on two-time correlation functions, especially its effect on final state amplitudes, was considered recently by simple modeling.[60] Thereby, it was shown that, as a function of t_p, in spin-alignment spectra of coupled ^{7}Li nuclei central components will show up with apparent phases differing from those of the satellite contributions.

V. EXPERIMENT

Polycrystalline h-$Li_{0.7}TiS_2$ had been prepared by Schöllhorn and Payer[30] starting from TiS_2 which was obtained via standard solid state chemistry procedures. A mixture of titanium and sulfur powders in the ratio 1:2.1 was heated at 870 K for about 2 weeks in an evacuated quartz tube. Excess sulfur was removed at 420 K under vacuum. Li was intercalated at room temperature in inert gas atmosphere using n-butyl lithium. The sample was characterized by x-ray diffraction and ^{7}Li NMR spectroscopy. Further details of sample preparation, especially for the host material h-TiS_2, are reported elsewhere.[27,77] The final product was sealed in a quartz tube under vacuum. It is fully homogenized concerning the Li distribution between the TiS_2 layers. The same sample was used before as a model substance in a comparative NMR relaxation study of hexagonal and cubic Li_xTiS_2.[30]

Spin-alignment echoes as well as spin-lattice (T_1^{-1}) and spin-spin relaxation rates (T_2^{-1}) were recorded at radio frequencies ranging from 39 to 155 MHz. The results are compared with spin-lattice relaxation data in the laboratory frame (T_1^{-1}) which had been measured by our group before in the frequency range from 10 to 39 MHz.[30,77,78] Furthermore, the new results from multiple-time NMR are compared with spin-lattice relaxation rates in the rotating frame ($T_{1\varrho\mathrm{diff}}^{-1}$), which had been measured at effective locking frequencies $\omega_{1\mathrm{eff}}/2\pi=2.1$, 5.2, and 10 kHz on the same sample by our group earlier.[30,77] The latter ones were acquired using the well-known spin-lock technique introduced by Redfield[43] and first applied by Ailion and Slichter[44] and Look and Lowe.[45]

Spin-alignment data and relaxation rates at 155 MHz were collected with a Bruker MSL 400 spectrometer connected to a shimmed Oxford cryomagnet at a fixed field of 9.4 T with a high homogeneity of the external magnetic field B_0. All the measurements at lower magnetic fields B_0 were carried out with a modified Bruker MSL 100 console in connection with a field-variable (0–8 T) Oxford cryomagnet.[79]

^{7}Li spin-alignment echoes as a function of mixing time t_m ($10\ \mu s \leqslant t_m \leqslant 100$ s) and for various evolution times t_p were measured using the three pulse Jeener-Broekaert sequence (see above). The recycle delay was at least $5T_1$. The 90° pulse length was about 4.5 μs ensuring a nonselective excitation of both the central and satellite transitions. Appropriate phase cycling[21,59] was employed in order to pick out the correct coherence pathway and to eliminate unwanted coherences as well as to decrease the effects of pulse imperfections. Spin-lattice relaxation rates T_1^{-1} were acquired using the well-known classical NMR methods such as the saturation recovery and/or the inversion recovery experiment.[80] Both methods yielded the same results. Spin-spin relaxation times T_2 were obtained by the solid echo technique[80] $64° - t_e - 90° - t$ with $10\ \mu s \leqslant t_e \leqslant 100\ \mu s$.

VI. RESULTS AND DISCUSSION

A. ^{7}Li spin-alignment echo NMR

1. Two-time correlation functions

Two-time sin-sin correlation functions $S_2(t_p,t_m)$ vs mixing time t_m ranging from 10 μs to 100 s were recorded for fixed evolution times t_p between 140 and 220 K. In Fig. 3, a typical decay of normalized ^{7}Li alignment echo amplitudes $S_2(t_p,t_m,t)$ sampled at $t=t_p=15$ μs and $T=193$ K is shown. The correlation function was measured at a Larmor frequency of $\omega_0/2\pi=155$ MHz. The echo decay proceeds in two clearly distinguishable steps in the whole investigated temperature range. The first step leading to a finite plateau value S_∞ at intermediate mixing times represents directly ionic jumps between electrically inequivalent sites in h-$Li_{0.7}TiS_2$. The second step leading from the plateau value to $S_{0,\infty}=0$ reflects an echo decay simply induced by longitudinal relaxation because the time constant of this decay step $T_{1\mathrm{SAE}}$ and its temperature behavior (140–220 K) is very similar to the spin-lattice relaxation time T_1 measured independently by standard NMR relaxation experiments such as the inversion or saturation recovery techniques. Additionally, according to the magnetization transients of the corresponding ^{7}Li NMR relaxation experiments the second S_2 step shows a purely exponential decay, whereas the first decay

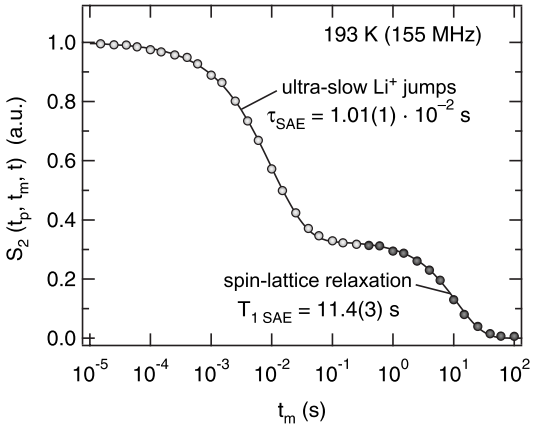

FIG. 3. Decay of the spin-alignment echo amplitudes S_2 of h-$Li_{0.7}TiS_2$ at 193 K as a function of mixing time t_m ($10\ \mu s \leqslant t_m \leqslant 100$ s) at a Larmor frequency of 155 MHz. The echoes were sampled at $t_p=15\ \mu s$. The decay is due to two processes: (i) ultraslow Li motions with a jump rate τ_{SAE}^{-1} of about 100 s^{-1}. The second decay step is induced by spin-lattice relaxation. The decay constant $T_{1SAE}=11.4(3)$ s is equal to that measured independently by a saturation recovery experiment, $T_1=11.8(1)$ s.

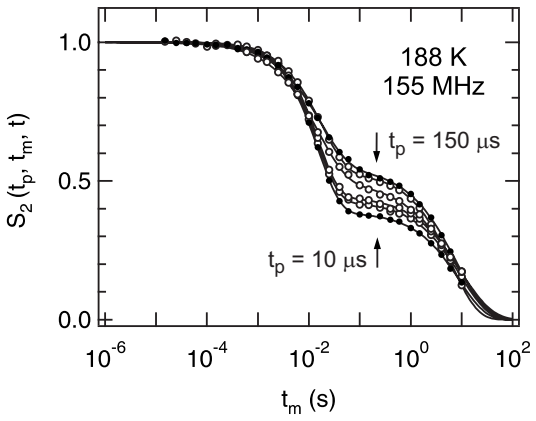

FIG. 4. sin-sin two-time correlation functions S_2 of h-$Li_{0.7}TiS_2$ for different evolution times t_p from 10 to 150 μs and constant mixing time of $t_m=10\ \mu s$. Data were recorded at 188 K and 155 MHz. The decay constants τ_{SAE}^{-1} and T_{1SAE}^{-1}, characterizing the first and second decay steps, respectively, are independent of t_p.

step has to be described with a slightly stretched exponential function,

$$S_2(t_p,t_m) = (1-S_\infty)\exp\left[-\left(\frac{t_m}{\tau_{SAE}}\right)^{\alpha}\right] + S_\infty \exp\left(-\frac{t_m}{T_{1SAE}}\right) + S_{0,\infty}. \quad (4)$$

A fit according to Eq. (4) is represented by the solid line in Fig. 3. In this example, the two-time constants are $\tau_{SAE}=1.01(1)\times 10^{-2}$ s and $T_{1SAE}=11.4(3)$ s, respectively. The stretching exponent α is 0.8(1) at 193 K. It will be shown below that τ_{SAE} is identical to the motional correlation time τ of the hopping process in $Li_{0.7}TiS_2$.

Interestingly, the relatively high plateau value S_∞ of about 0.3 at 193 K, although recorded at short t_p, already indicates that only a small number of electrically inequivalent sites are involved in the Li diffusion process in h-$Li_{0.7}TiS_2$. In general, the (normalized) final state correlation $S_\infty(t_p\rightarrow\infty)$ can be regarded from the perspective of neutron scattering as a generalized elastic incoherent structure factor (EISF).[81] The amplitude of $S_\infty(t_p)$ is expected to be independent of t_m for large t_p, whereas $S_\infty=f(t_p)$ and $S_\infty(t_p\rightarrow\infty)$ depends on the type of translation (as well as reorientation) process. For an N-site jump process, EISF is expected to equal $1/N$ if the N Li sites equally participate in the diffusion process.[21] Regarding the crystal structure of hexagonal Li_xTiS_2, only two available and crystallographically inequivalent sites for Li^+ between the van der Waals layers can be identified (see Fig. 1). The ions reside preferentially in octahedral sites ($1b$) characterized by a quadrupole coupling constant δ_o of about $\delta_o=14$ kHz (293 K) as obtained from the satellite positions of the ^{7}Li NMR spectra.[82] The quadrupole coupling constant δ_t of the tetrahedral site ($2d$) is experimentally difficult to measure because of the very low occupation of the $2d$ sites by lithium ions although the number of tetrahedral sites is three times larger than the number of available octahedral positions. From density functional calculations, the coupling constant was found to be larger by about a factor of 3 than that of the octahedral site.[82] It was suggested that the $2d$ position is a transition structure of the diffusion process[37] (see above). Assuming that the Li ion passes the tetrahedral site while jumping from an octahedral site to a vacant one ($1b\rightarrow 2d\rightarrow 1b'$), the associated fluctuations of ω_Q would lead to an echo decay with a final state amplitude S_∞ of 1/2. In order to measure $S_\infty(t_p\rightarrow\infty)$, we have recorded two-time correlation functions vs evolution times up to about 150 μs (Fig. 4). The decay constant τ_{SAE}^{-1}, as well as that of the second decay step T_{1SAE}^{-1}, is independent of t_p as can be seen simply from the positions of the S_2 curves in Fig. 4. The fact that τ_{SAE}^{-1} being obtained at the relatively short evolution time $t_p=10\ \mu s$ is identical to those values found at longer times t_p means that already at short t_p all Li jumps are detected. Additionally, this fact reveals that the involved quadrupole frequencies differ largely from each other (as also found by the calculations in Ref. 82, see above) because with the choice of t_p the sensitivity to changes in ω_Q is set. The larger t_p, the better small changes in $\omega_Q(t_m)$ can be detected because the difference of the associated phases $\sin[\omega_Q(0)t_p]$ and $\sin[\omega_Q(t_m)t_p]$ will become better visible with increasing t_p if $\omega_Q(0)t_p \approx \omega_Q(t_m)t_p$. Simultaneously, a possible $\tau_{SAE}^{-1}(t_p)$ dependence should be accompanied by a decrease of the final state amplitude S_∞ with increasing t_p. This is not the case here. In Fig. 5, the S_∞ values from the correlation functions in Fig. 4 are shown vs t_p. For t_p values above 100 μs, a limiting value of 1/2 is reached pointing out the presence of the above mentioned two-site jump process in hexagonal h-$Li_{0.7}TiS_2$. Obviously, Li sites with quite different quadrupole frequencies are involved which can be identified as the octahedral and tetrahedral positions between the TiS_2 layers. The results of Figs. 4 and 5 hold also for other temperatures.

It has to be mentioned that, especially for spin-3/2 probes, the final state amplitude may be additionally affected

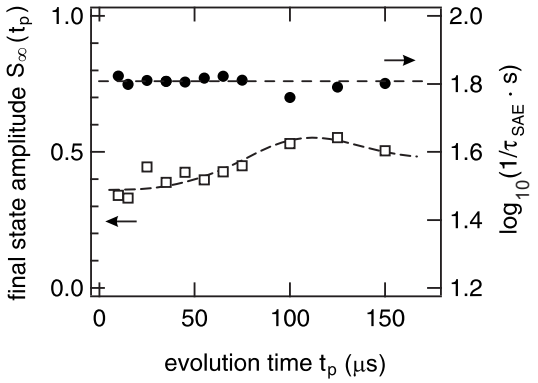

FIG. 5. Evolution time dependence of the final state amplitude S_∞ (□) recorded at t_m=10 μs, 188 K, and 155 MHz. The t_p dependence of the corresponding SAE decay rate τ_{SAE}^{-1} (●) is also shown.

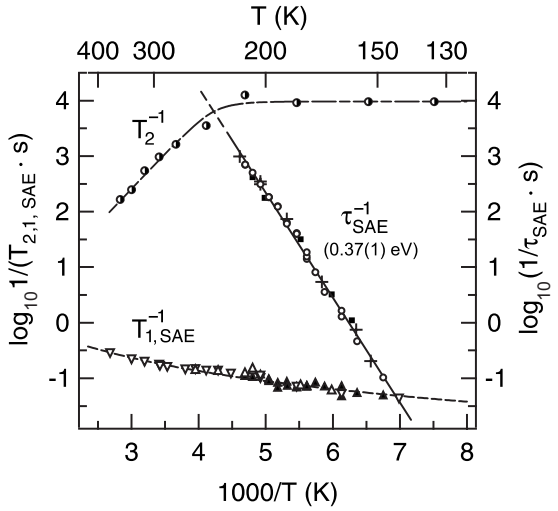

FIG. 6. Li jump rates τ_{SAE}^{-1} (right-hand ordinate) from spin-alignment echo NMR recorded at two radio frequencies [77.7 MHz (■) and 155 MHz (○)] and two different evolution times [155 MHz, t_p=10 μs (+) and t_p=15 μs (○)] vs reciprocal temperature. For comparison, spin-spin relaxation rates T_2^{-1} [77.7 MHz (◑)] and spin-lattice relaxation rates T_1^{-1} [77.7 MHz (▽) and 155 MHz (△)] are shown, too (left-hand ordinate). In contrast to τ_{SAE}^{-1}, spin-lattice relaxation is not induced by Li diffusivity in this T range. The decrease of T_2^{-1} above 240 K indicates a Li jump rate larger than 10^{-3} s^{-1} which is in good agreement with τ_{SAE}^{-1} when extrapolated to higher T. The solid line fitted to the τ_{SAE}^{-1} values yields an activation energy of 0.37(1) eV. Decay rates $T_{1\,SAE}^{-1}$ (▲) agree well with the independently measured spin-lattice relaxation rates T_1^{-1}.

by the number of effectively dipolarly coupled ^{7}Li spins.[59] The more spins are effectively coupled the smaller would be the plateau value. The dipole-dipole interaction is much weaker than the quadrupole interaction in h-$Li_{0.7}TiS_2$. Dipolar contributions are increasingly stored the larger t_p is chosen. Thus, one could imagine that with increasing t_p, the plateau values continually decrease also because of dipole-dipole contributions. As this is not observed here, we conclude that the separation of quadrupolar from dipolar order is sufficiently good in h-$Li_{0.7}TiS_2$ so that dipolar interactions do not play an important role in echo formation. In fact, the central line in the corresponding ^{7}Li spin-alignment spectra is almost fully suppressed.[32]

2. Comparison with results from relaxation NMR below 220 K

In Fig. 6, the SAE NMR decay rates τ_{SAE}^{-1} recorded at different external magnetic fields and evolution times t_p =10 μs and t_p=15 μs are shown in an Arrhenius plot in comparison with the T_1^{-1} and T_2^{-1} results below 400 K. It is helpful to check the dependence on B_0 in order to find out if τ_{SAE} can be really identified with the motional correlation time τ which is expected to be independent of the Larmor frequency $\omega_0/2\pi$. In the present case, $\tau_{SAE} \neq f(\omega_0)$ is fulfilled between 10.0 and 155 MHz, being the frequency range covered here. Any field dependence of τ_{SAE} would give rise to the assumption that the S_2 decay is additionally influenced by spin-lattice relaxation which depends, when induced by diffusion, on the applied Larmor frequency used to measure the longitudinal recovery of the magnetization. Additionally, this possibility can be ruled out in the present case because a clear separation of τ_{SAE}^{-1} from longitudinal relaxation effects was already possible via the discrimination of the two time constants describing the S_2 curves. The characteristic rates $T_{1\,SAE}^{-1}$ of the second decay step are nearly identical to the independently measured T_1^{-1} ^{7}Li NMR relaxation rates, i.e., we have $T_{1\,SAE}^{-1}=T_1^{-1}$. Moreover, T_1^{-1} and τ_{SAE}^{-1} can be clearly differentiated via their completely different temperature behavior. The τ_{SAE}^{-1} rates show a strong dependence on T yielding an activation energy of slow Li jump processes of 0.37(1) eV. In contrast to that, ^{7}Li NMR longitudinal relaxation (T_1^{-1}) is *not* induced by Li diffusion in this low-temperature range at all. The characteristic frequency dependent diffusion induced rate peak $T_1^{-1}(1/T)$, recorded at, e.g., $\omega_0/2\pi$=77.7 MHz, shows up above 400 K (see Fig. 10 and see the data point at the highest temperature). Thus, the spin-lattice relaxation rates shown in Fig. 6 reflect a nondiffusive relaxation background, i.e., $T_1^{-1}=T_{1\,bgr}^{-1}$ (see Sec. VI B 2 for a possible explanation of this background contribution).

In addition to the influence of longitudinal relaxation on τ_{SAE}^{-1} that of spin-spin-relaxation (T_2^{-1}) should also be considered. As shown in Fig. 6, below 220 K spin-spin relaxation rates are independent of T $[d(\ln T_2)/d[1/(k_BT)]=0]$, whereas τ_{SAE}^{-1} strongly depends on T. A value of the order of T_2^{-1} $=10^4$ s^{-1} is in good agreement with earlier results reported in the literature[15] for h-$Li_{0.7}TiS_2$. In this so-called "rigid-lattice regime," the Li jump rate is far away from the value of the inverse line width ($\langle\Delta\omega^2\rangle\tau^2 \gg 1$, $\langle\Delta\omega^2\rangle$ being the dipolar second moment) and τ_{SAE}^{-1} is not affected by transverse relaxation (T_2^{-1}). At about 240 K, motional averaging of local magnetic fields sets in and, therefore, the width of the corresponding resonance line starts to narrow. Accordingly, the T_2^{-1} rates decrease. Roughly speaking, motional narrowing starts when the jump rate reaches a value of the order 10^3 s^{-1}. This is in good agreement with the τ_{SAE}^{-1} values: At about 220 K, we obtained a Li residence time τ_{SAE} of about 1 ms.

As expected, in the rigid-lattice regime, i.e., below T =220 K in the case of h-$Li_{0.7}TiS_2$, neither the measurement of T_2^{-1} nor that of T_1^{-1} is helpful to detect extremely slow Li

jumps. However, by applying ^{7}Li spin-alignment echo NMR to temperatures below 220 K, it was possible to trace extremely slow ionic jumps covering a dynamic range of about four decades, i.e., $10^{-1} \leqslant \tau_{SAE}^{-1} \leqslant 10^3$ s^{-1}.

B. Diffusion induced relaxation NMR: Comparison with results from stimulated echoes

1. Spin-spin relaxation

Temperature dependent spin-spin relaxation data T_2^{-1} recorded at $\omega_0/2\pi=77.7$ MHz are shown in Fig. 6 (see above). Below 220 K, spin-spin relaxation rates are temperature independent and are of the order of 10^4 s^{-1} as expected for ^{7}Li. After the beginning of motional narrowing at about 240 K, the rates become smaller reaching a value of $T_2^{-1} \approx 10^2$ s^{-1} at 350 K. The corresponding activation energy E_A is larger than the value of the slope $d(\ln T_2)/d[1/(k_B T)]=0.25(2)$ eV of the T_2^{-1} values above 250 K. Taking into account the dimensionality ($d=2$) of the Li diffusion process in h-$Li_{0.7}TiS_2$, according to Ref. 83, the following relation holds:

$$\frac{d \ln T_2}{d1/(k_B T)} = -E_A \left\{ 1 + \left(\frac{E_A}{k_B T} + \frac{1}{2} \ln(\langle \Delta\omega^2 \rangle \tau_0^2) \right) \right\}. \quad (5)$$

Here, $\langle \Delta\omega^2 \rangle$ is the dipolar second moment and τ_0^{-1} the preexponential factor of the corresponding Arrhenius relation $\tau^{-1}=\tau_0^{-1} \exp[-E_A/(k_B T)]$. Taking $\tau_0^{-1}=6.3(1)\times 10^{12}$ s^{-1} from the result to be presented in Sec. VI C, an activation energy $E_A=0.36(2)$ eV is estimated in close agreement with the value obtained from SAE NMR and from spin-lattice relaxation in the laboratory and rotating frame [see Secs. VI A 2 and VI B (below)].

Extrapolating the spin-spin relaxation rates measured at $\omega_0/2\pi=77.7$ MHz to temperatures higher than 500 K where the corresponding T_1^{-1} maximum shows up ("extreme narrowing case" $\omega_0\tau \ll 1$), it is found that the T_2^{-1} rates are much larger than the T_1^{-1} rates at the same temperature. Contrary to the standard behavior $T_2^{-1}=T_1^{-1}$ for $\omega_0\tau \ll 1$ (see, e.g., Ref. 23), $T_1/T_2 > 1$ occurs and is expected because of the anomalously large secular (independent of ω_0) contribution to T_2^{-1} for low dimensions ($d=1$ or 2).[83]

2. ^{7}Li NMR spin-lattice relaxation in the laboratory and rotating reference frame

Transitions between energy levels of the spin system may be induced by internal magnetic or electric fluctuating fields. Longitudinal NMR relaxation will be effectively induced by atomic diffusion when the spectral density function $J(\omega)$ has components at the transition frequencies. $J(\omega)$ is a function of the correlation rate τ_c^{-1}, being directly related to the jump rate τ^{-1} of the atomic diffusion process, and thus a function of inverse temperature T, because

$$\tau_c^{-1} \cong \tau^{-1} = \tau_0^{-1} \exp(-E_A/k_B T). \quad (6)$$

$J(\omega)$ is the Fourier transform of the correlation function $G(t)$ containing the temporal information about the diffusion process characterized by τ_c. At a certain temperature and a given frequency ω_0, T_1^{-1} will be maximal indicating that τ reaches the range of the inverse Larmor frequency, i.e., $\tau\omega_0 \approx 1$. Thus, T_1^{-1} measurements are sensitive to ionic motions with jump rates of the order of the Larmor frequency applied, i.e., in the megahertz range. For $\omega_0\tau \ll 1$ and $\omega_0\tau \gg 1$, longitudinal relaxation is much less effective, which is why diffusion induced spin-lattice relaxation has been looked at as an "internal resonance" phenomenon.[23] The resulting diffusion induced relaxation maxima with its characteristic flanks on the low-($\omega_0\tau \gg 1$) and high-temperature sides ($\omega_0\tau \ll 1$) are often expected to appear at high temperatures for Li conductors with moderate cation diffusivity. The measurement of relaxation rate peaks at various frequencies $\omega_0/2\pi$ offers the possibility to shift the maxima to higher and lower values of T and, therefore, to scan $\tau^{-1}=f(1/T)$, i.e., to obtain pairs of variates $(\tau^{-1}, 1/T)$ fulfilling Eq. (6).

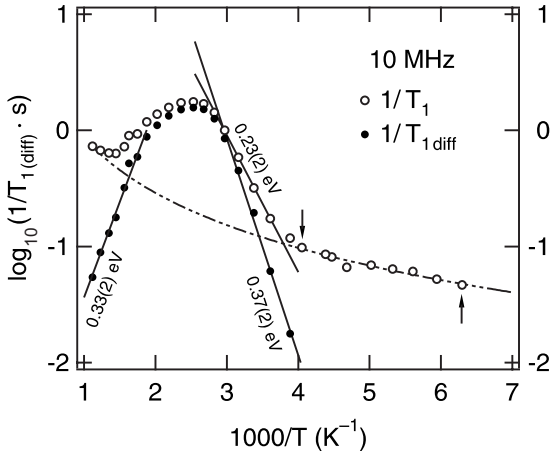

FIG. 7. Overall ^{7}Li NMR spin-lattice relaxation rates T_1^{-1} (○) of h-$Li_{0.7}TiS_2$ as a function of inverse temperature. Data were partly taken from Ref. 30. Values were recorded at $\omega_0/2\pi=10.0$ MHz. Below 250 K only a nondiffusive background rate $T_{1\,bgr}^{-1}$ shows up which is fitted by a power law just between the measured rates marked with two arrows and subsequently extrapolated to higher T (dashed dotted line). At the highest temperatures, where $T_{1\,diff}^{-1} \ll T_{1\,bgr}^{-1}$, the background rate shows up once again and coincides with the extrapolated data indicating a proper choice of extrapolation. The corresponding purely diffusion induced rates $T_{1\,diff}^{-1}$ (●) are obtained by subtracting the extrapolated values of $T_{1\,bgr}^{-1}$ from T_1^{-1}. The low-T flank of the peak $T_{1\,diff}^{-1}(1/T)$ finally yields $E_A=0.37(2)$ eV for the Li hopping process.

^{7}Li spin-lattice relaxation rates T_1^{-1} of h-$Li_{0.7}TiS_2$ at a relatively low Larmor frequency of 10.0 MHz are shown as a function of inverse temperature in Fig. 7. Data were partly taken from Ref. 30. The characteristic relaxation rate maximum shows up around $T=415$ K. Below 250 K, Li jump rates in h-$Li_{0.7}TiS_2$ are too small ($\omega_0\tau \gg\gg 1$) to affect longitudinal relaxation at this frequency significantly. In this temperature range, Li diffusion is not the origin of spin-lattice relaxation. Instead, it is caused by other types of background relaxation mechanisms due to spin fluctuations of paramagnetic impurities and lattice vibrations and/or due to coupling of the ^{7}Li nuclei with conduction electrons. Therefore, the effective background rate is given by a superposition of the different relaxation rates with their characteristic temperature (and frequency) dependencies,

$$T_{1\mathrm{bgr}}^{-1} = aT_{1\mathrm{para}}^{-1} + bT_{1\mathrm{phonon}}^{-1} + cT_{1\mathrm{elec}}^{-1} + \cdots, \quad (7)$$

with $a,b,c,\ldots$ being the respective weighting factors. Here, the resulting effective (and weaker than activated) temperature dependence of $T_{1\ \mathrm{bgr}}^{-1}$ can be all in all described by a power law $T_{1\ \mathrm{bgr}}^{-1} \propto T^{\kappa}$, with $\kappa = 1.56(2)$ (see Fig. 7). Presumably, in h-$Li_{0.7}TiS_2$ relaxation via coupling with conduction electrons plays a more important role than the other mechanisms. Irrespective of the exact nature of background relaxation here, to obtain the pure diffusion induced rate $T_{1\ \mathrm{diff}}^{-1}$, the background relaxation has to be extrapolated to higher temperatures (dashed dotted line in Fig. 7) and subtracted from the overall rate T_1^{-1}. For this correction procedure (see Fig. 7), the power law was fitted to the relaxation rates between 160 and 250 K and after that extrapolated to about 900 K. Interestingly, above 750 K, the same relaxation background as observed at low T shows up again and coincides with the performed fit. This indicates a proper ansatz for fitting and extrapolation. This analysis shows clearly that the background relaxation rate is superimposed by an Li diffusion induced spin-lattice relaxation rate peak. Comparing the slopes of the low-T flanks of the overall (T_1^{-1}) and purely diffusion induced rates ($T_{1\ \mathrm{diff}}^{-1}$) recorded at 10.0 MHz (Fig. 7), the activation energy increases from 0.23(2) to 0.37(2) eV. This illustrates the influence of the background contribution to T_1^{-1} and demonstrates clearly that it has to be considered for a meaningful data analysis. The value of $E_A = 0.37(2)$ eV at 10.0 MHz is in perfect agreement with the corresponding activation energy obtained from stimulated echo NMR at much lower temperatures.

Careful background correction is particularly important at higher Larmor frequencies. Increasing $\omega_0/2\pi$ to values up to 77.7 MHz shifts the position of the rate peak $T_{1\ \mathrm{diff}}^{-1}(1/T)$ toward higher temperatures. Simultaneously, the $T_{1\ \mathrm{diff}}^{-1}(1/T)$ rates decrease, whereas the background contribution to T_1^{-1} is nearly unchanged. Therefore, at the highest frequencies, the high-T and low-T flanks of the rate maximum are no longer well detectable because $T_{1\ \mathrm{diff}}^{-1}(1/T)$ becomes much smaller than $T_{1\ \mathrm{bgr}}^{-1}(1/T)$. As a consequence, a reliable separation of diffusion induced contributions from the overall spin-lattice relaxation rates T_1^{-1} at frequencies higher than 77.7 MHz is no longer possible. At 155 MHz, for example, the diffusion induced rate maximum is too shallow in order to be clearly distinguishable from the relaxation background. This circumstance marks the upper limit of measuring jump rates by ^{7}Li relaxation NMR in the present case. For the NMR relaxation measurements in the laboratory frame, the most reliable results were obtained at Larmor frequencies between 10 and 77.7 MHz, whereas for those performed in the rotating frame, the background effects are expected to show no or only a weak influence on $T_{1\rho\ \mathrm{diff}}^{-1}$ recorded near the rate maximum.

In Fig. 8, typical rotating frame spin-lattice relaxation rates $T_{1\rho\ \mathrm{diff}}^{-1}(1/T)$ are displayed. The data were recorded at a locking frequency of $\omega_1/2\pi = 5.2$ kHz using an external magnetic field B_0 corresponding to $\omega_0/2\pi = 77.7$ MHz. Additionally, in Fig. 8, the purely diffusion induced rates $T_{1\ \mathrm{diff}}^{-1}(1/T)$ at $\omega_0/2\pi = 10.0$ MHz are shown. As expected,

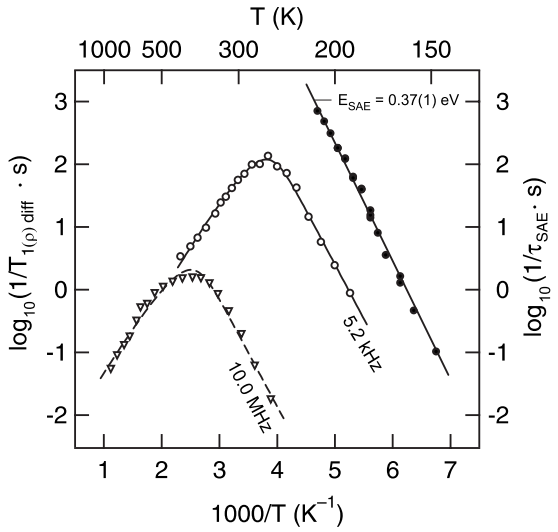

FIG. 8. ^{7}Li spin-alignment decay rates τ_{SAE}^{-1} (●, $t_p = 15$ μs) as a function of inverse temperature (right-hand ordinate). The rates are independent of ω_0. The solid line corresponds to $E_A^{\mathrm{SAE}} = 0.37(1)$ ev. For comparison, the asymmetric diffusion induced peaks $T_{1\mathrm{diff}}^{-1}(1/T)$ (▽) and $T_{1\rho\mathrm{diff}}^{-1}(1/T)$ (○) recorded at $\omega_0/2\pi = 10.0$ MHz and $\omega_1/2\pi = 5.2$ kHz, respectively, are shown, too (data partly taken from Ref. 30). The fits to the relaxation data take account of 2D Li diffusion in h-$Li_{0.7}TiS_2$ according to Richards' equation [see Eq. (9)].

the absolute rates $T_{1\rho}^{-1}$ are much higher than those recorded in the laboratory frame in the same temperature range. Background relaxation rates were similar in both cases. Thus, for the rotating frame data, a background correction has no influence on the rates $T_{1\rho}^{-1}$ even at higher temperatures, i.e., $T_{1\rho\ \mathrm{diff}}^{-1} = T_{1\rho}^{-1}$. Whereas the maximum of the laboratory frame relaxation peak $T_{1\ \mathrm{diff}}^{-1}(1/T)$ recorded at 10.0 MHz shows up at around 415 K, the diffusion induced maxima of the corresponding peaks in the rotating reference frame, being similar in shape to the $T_{1\ \mathrm{diff}}^{-1}(1/T)$ peak, are shifted toward lower temperatures due to the much smaller locking frequency $\omega_1/2\pi$ compared to $\omega_0/2\pi$.

For comparison, Li jump rates obtained from the first decay step of the two-time correlation functions $S_2(t_p = 15\ \mu\mathrm{s}, t_m)$ are shown in Fig. 8, too. Without any detailed analysis of the diffusion induced relaxation rate peaks, the parallel trend of the low-temperature flanks of the rate peaks compared to the temperature behavior of the spin-alignment decay rates indicates already that all three techniques probe the same Li hopping process in $Li_{0.7}TiS_2$. Fitting just the low-T flank of the relaxation peaks according to an Arrhenius relation yields $E_A^{\text{low-}T} = 0.37(2)$ eV for $T_{1\ \mathrm{diff}}^{-1}(1/T)$ (see above) and $E_A^{\text{low-}T} = 0.37(1)$ eV for $T_{1\rho\ \mathrm{diff}}^{-1}(1/T)$. For comparison, E_A^{SAE} is 0.37(1) eV. Similar results for $E_A^{\text{low-}T}$ were obtained from spin-lattice relaxation NMR measurements performed at other frequencies, e.g., $\omega_0/2\pi = 27$, 38, and 77.7 MHz, and at $\omega_1/2\pi = 2.1$ kHz as well as 10 kHz.

As expected for an ideal 2D ionic conductor (see next section) the $T_{1\rho\ \mathrm{diff}}^{-1}(1/T)$ rate peaks are *not* symmetric and show a reduced slope on the high-T side. Fitting both flanks using an Arrhenius relation reveals that the activation energy

of the high-T side E_A^{high} is only 0.29(1) eV at 5.2 kHz. This is about $0.78E_A^{low}$, which is in good agreement with the expression introduced by Richards [see Eq. (9), next section] for the spectral density function of 2D diffusion revealing that the high-temperature slope is about $0.77E_A$.

3. Spectral density for a two-dimensional ionic conductor

The spectral density $J(\omega,\tau)$, determining the frequency and temperature dependence of the relaxation rate $T_{1(\rho)\text{diff}}^{-1}$, for three-dimensional (3D) translational diffusion is given by the well-known phenomenological expression introduced by Bloembergen-Purcell-Pound (BPP),[84]

$$J(\omega,\tau) \propto \frac{\tau}{1+\omega^2\tau^2}. \tag{8}$$

Standard BPP behavior relies on a single Lorentzian spectral density $J(\omega,\tau)$ according to a single exponentially decaying correlation function $G(t)$ resulting in a symmetric $T_{1\text{diff}}^{-1}(1/T)$ peak. The BPP model and other theoretical approaches show the same dependencies of $J(\omega,\tau)$ in the low-temperature limit $[\omega\tau \gg 1, J(\omega,\tau) \propto \tau^{-1}\omega^{-2}]$ and in the high-temperature limit $[\omega\tau \ll 1, J(\omega,\tau) \propto \tau]$.

In contrast to 3D diffusion, the characteristic $T_{1\text{diff}}^{-1}(1/T)$ peak in the case of two-dimensional (2D) diffusion is *not* symmetric.[85] Instead, the high-T flank reveals a lower slope compared to that in the low-temperature range. Additionally, a logarithmic frequency dependence of the relaxation rates on the high-temperature side shows up, whereas for 3D systems, no frequency dependence is expected.[23] In order to describe the temperature and frequency dependence of the NMR relaxation rates for a 2D system such as h-$Li_{0.7}TiS_2$, the two limiting cases for low $[\omega\tau \gg 1 : J(\omega,\tau) \propto \omega^{-2}\tau^{-1}$ (see low-T BPP limit)] and high temperatures $[\omega\tau \ll 1 : J(\omega,\tau) \propto \tau \ln(1/\omega\tau)]$ are combined by Richards[85] in the empirical expression,

$$J(\omega,\tau) \propto \tau \ln\left(1+\frac{1}{(\omega\tau)^\beta}\right), \quad \beta = 2. \tag{9}$$

In a good approximation, the frequency and temperature dependencies of $T_{1\rho\text{diff}}^{-1}$ are then described by a single function $J(\omega_0,\tau)$. Equation (9) leads to asymmetric diffusion induced relaxation rate peaks with the high-T slope ($\omega\tau \ll 1$) being reduced by about 25% compared to that in the limit $\omega\tau \gg 1$. β expresses the frequency dependence of the relaxation rate. $\beta=2$ is expected for BPP behavior. Taking into account correlation effects resulting from Coulomb interactions of the hopping ions and/or structural disorder, an exponent $\beta<2$ is expected resulting in a smaller slope of the low-T side, i.e., in the limit $\omega\tau \gg 1$. Values of $\beta<2$ can be explained by various relaxation models developed for 3D systems by Funke[86] and by Ngai,[87] for example.

Fits according to Richards' expression [Eq. (9)] are shown in Fig. 8 for two relaxation rate peaks $T_{1\text{diff}}^{-1}(1/T)$ and $T_{1\rho\text{diff}}^{-1}(1/T)$ recorded at 10.0 and 5.2 kHz, respectively. The $T_{1\rho\text{diff}}^{-1}$ fits for $\beta \leqslant 2$ yield activation energies E_A between 0.35 and 0.38 eV (see Table I). These values are in very good agreement with those which were obtained by fitting just the low-T side according to an Arrhenius law (see Sec. IV B 2). Without restrictions for β its value lies in the range $1.9 \leqslant \beta \leqslant 2.1$ with nearly no effect on E_A. Forcing β to be equal to or smaller than 2, all the $T_{1\rho\text{diff}}^{-1}(1/T)$ fits gave $1.9 \leqslant \beta \leqslant 2.0$. Therefore, there are no indications that the diffusion process is intensively influenced by disorder and/or correlation effects.

TABLE I. Results from fits according to the Richards expression [Eq. (9)]. The fit of the $T_{1\rho}^{-1}(1/T)$ data at 5.2 kHz is exemplarily shown in Fig. 8. β was always restricted to be equal to or smaller than 2.

$\omega_{\text{eff}}/2\pi$ (kHz)	E_A (eV)	τ_0^{-1} (s^{-1})	$\beta \leqslant 2$
2.1	0.35(1)	$2(1)\times10^{11}$	2.0
5.2	0.35(1)	$3(1)\times10^{11}$	2.0
10.0	0.38(1)	$2(1)\times10^{12}$	1.9

It is noted that for NMR spin-lattice relaxation measurements in the rotating frame local magnetic fields $B_{1\text{loc}}$ have to be taken into account. This is because of the much lower locking field B_1 compared to the external magnetic field B_0 being effective for T_1 relaxation in the laboratory frame ($B_1 \ll B_0$). Consequently, ω_1 was replaced by

$$\omega_{\text{eff}} = \gamma\sqrt{B_1^2 + B_{1\rho\text{loc}}^2}, \tag{10}$$

where $B_{1\rho\text{loc}}$ was estimated by a spin-echo experiment to be about $B_{1\text{loc}}/\sqrt{3} = 0.76(2)\times10^{-4}$ T.[77]. γ is the magnetogyric ratio of a ^{7}Li nucleus.

The corresponding fits to the peaks $T_{1\text{diff}}^{-1}(1/T)$ measured in the laboratory frame yield similar results as obtained in the rotating frame experiments. For instance, the fit in Fig. 8 shown for $\omega_0/2\pi = 10.0$ MHz is determined by $E_A = 0.34(2)$ eV and $\tau_0^{-1} = 2(1)\times10^{12}$ s^{-1} if β is restricted to be smaller than or equal to 2. Without restrictions β turned out to be 2.01(1), i.e., slightly above 2, once again with no influence on E_A and τ_0^{-1}. In Table II, the results for the activation energies from the different methods are summarized. Values of E_A obtained by fitting just the low-T flanks of the corresponding rate peaks are also included.

Besides the analysis of the temperature behavior of the relaxation rate, the parameter β is directly obtainable by recording $T_{1\text{diff}}^{-1}$ at different magnetic fields for which $\omega\tau \gg 1$ holds.[23] ^{7}Li spin-lattice relaxation rates measured at different angular frequencies $\omega_0 = \nu_0 2\pi$ and various temperatures on the low-T flank of the corresponding relaxation peaks are shown in Fig. 9. Between $\nu_0 = 10$ and 39 MHz, $\beta \approx 2$ is found confirming the value obtained from the temperature analysis of $T_{1\text{diff}}^{-1}$. At higher frequencies, i.e., at 77.7 and 155 MHz, the corresponding rates have a larger error because of the more difficult separation of background relaxation effects (see above). For this reason, the data at these frequencies were not taken into account in Fig. 9.

Whereas $\beta=2$ is found for $\omega_{0,1}\tau \gg 1$, the diffusion induced relaxation rates of h-$Li_{0.7}TiS_2$ in the laboratory as well as in the rotating frame reveal a logarithmic frequency dependence if $\omega_{0,1}\tau \gg 1$, i.e., on the high-T flank of the rate

TABLE II. Comparison of activation energies E_A and preexponential factors τ_0^{-1} for polycrystalline h-$Li_{0.7}TiS_2$ in various subranges of temperature obtained from different NMR methods.

NMR method	E_A (eV)		τ_0^{-1} (s^{-1})
SAE[a]	0.37(1)		$1(1\times10^{12})$
T_2[b]	0.36(2)		
	Low-T flank		2D Richards fit[c]
$T_{1\rho}$ (5.2 kHz)	0.37(1)[d]	0.35(1)	$3(1)\times10^{11}$
T_1 (10.0 MHz)	0.37(2)[e]	0.34(2)	$2(1)\times10^{12}$

[a]$140<T<220$ K (rigid-lattice regime)
[b]$250<T<360$ K.
[c]Fits according to Eq. (9) (see Fig. 8 for temperature ranges); the exponent β was restricted to be smaller than or equal to 2 (see text for further details).
[d]$190<T<240$ K, (low-T flank of the $T_{1\rho\mathrm{diff}}^{-1}(1/T)$ peak).
[e]$260<T<340$ K, (low-T flank of the $T_{1\mathrm{diff}}^{-1}(1/T)$ peak).

peaks.[30] Thus, besides the temperature dependence of $T_{1\mathrm{diff}}^{-1}$ and $T_{1\rho\mathrm{diff}}^{-1}$, the 2D nature of Li diffusion in h-$Li_{0.7}TiS_2$ is confirmed also via the frequency dependence of the spin-lattice relaxation rates. To our knowledge, the layered polymorph of lithium titanium disulfide is the only Li conductor for which the two dimensionality of cation diffusion is probed in this way by frequency and temperature dependent ^{7}Li relaxation NMR, so far.

C. Comparison of Li jump rates from ^{7}Li SAE and relaxation NMR: Li diffusion pathway in $Li_{0.7}TiS_2$

In Fig. 10, the jump rates directly obtained from stimulated-echo decays at $t_p=15$ μs are shown together with those read out from the various diffusion induced spin-lattice

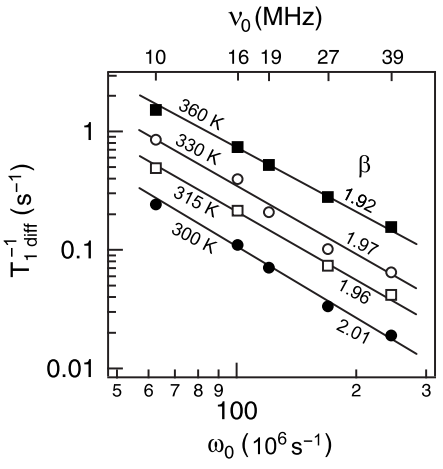

FIG. 9. Frequency dependence (low-temperature flank) of the diffusion induced relaxation rate. $\beta=2$ indicates that $T_{1\mathrm{diff}}^{-1}$ in h-$Li_{0.7}TiS_2$ follows simple BPP behavior in the case $\omega_0 \gg \tau^{-1}$. Relaxation rates were recorded at various temperatures in the range $\omega_0\tau \gg 1$.

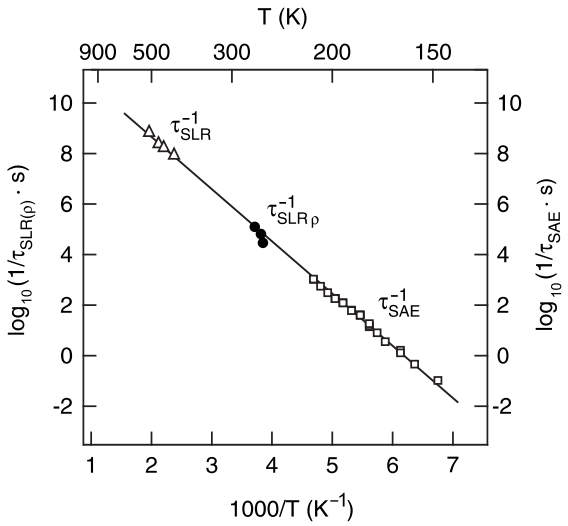

FIG. 10. Li jump rates of the 2D conductor h-$Li_{0.7}TiS_2$ vs reciprocal temperature. The τ_{SAE}^{-1} rates (□) were measured directly by means of ^{7}Li SAE NMR, whereas the rates τ_{SLR}^{-1} (△) and $\tau_{\mathrm{SLR}\rho}^{-1}$ (•) were deduced from the maxima positions of the corresponding rate peaks $T_{1\mathrm{diff}}^{-1}(1/T)$ and $T_{1\rho\mathrm{diff}}^{-1}(1/T)$, respectively (see partly Fig. 8). $T_{1\mathrm{diff}}^{-1}$ relaxation peaks were recorded at 10, 19.2, 27.9, and 77.7 MHz. The $\tau_{\mathrm{SLR}\rho}^{-1}$ rates were obtained from NMR spin-lattice relaxation experiments in the rotating frame at $\omega_{1\mathrm{eff}}/2\pi=2.1$, 5.2, and 10 kHz, respectively. The solid line corresponds to $E_A=0.41(1)$ eV and $\tau_0^{-1}=6.3(1)\times10^{12}$ s^{-1}.

relaxation rate peaks ($T_{1\mathrm{diff}}^{-1}$ and $T_{1\rho\mathrm{diff}}^{-1}$) at different Larmor and locking frequencies. The jump rates from relaxation NMR were determined via the maximum conditions $\omega_0\tau \approx 0.62$ for the $T_{1\mathrm{diff}}^{-1}$ peak and $\omega_1\tau \approx 0.55$ for the $T_{1\rho\mathrm{diff}}^{-1}$ peak, respectively. As can be clearly seen from Fig. 10, the jump rates from ^{7}Li SAE NMR—after extrapolation to higher temperatures—fit very well to those obtained by ^{7}Li spin-lattice relaxation NMR although both types of experiments probe *a priori* different correlation functions. Obviously, a solitary diffusion process is effective and responsible for the transport properties of h-$Li_{0.7}TiS_2$ in the entire investigated temperature range (148–510 K). By combining different NMR techniques, 2D Li diffusion in h-$Li_{0.7}TiS_2$ was investigated in a dynamic range of about 10 orders of magnitude, i.e., with jump rates ranging between 0.1 and 7.8×10^8 s^{-1}. Altogether, the rates follow an Arrhenius law with an activation energy of $E_A=0.41(1)$ eV and a preexponential factor of $\tau_0^{-1}=6.3(1)\times10^{12}$ s^{-1}. The latter one is in the typical range of phonon frequencies and corroborates once more that the measured rates are equal to Li jump rates. Quite recently, we have measured pre-exponential factors using ^{7}Li SAE NMR also for other Li conductors such as single-crystalline Li_3N ($\approx1\times10^{13}$ s^{-1}),[32] polycrystalline $Li_4Ti_5O_{12}$ [$4.9(1)\times10^{13}$ s^{-1}],[67] as well as for the high-T modification of Li_7BiO_6 (5×10^{12} s^{-1}).[88]

With ^{7}Li SAE NMR, only those Li jump processes can be detected which lead to changes of the corresponding quadrupole frequencies. Jumps directly between two octahedral sites in h-$Li_{0.7}TiS_2$ are not "seen" by SAE NMR since no change of the quadrupole frequency occurs. However, by

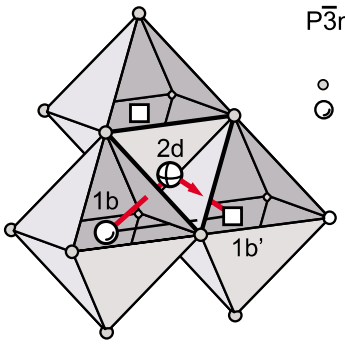

FIG. 11. (Color online) Li diffusion pathway in h-$Li_{0.7}TiS_2$ as probed by ^{7}Li spin-alignment echo NMR ($1b \rightarrow 2d \rightarrow 1b'$). The involvement of tetrahedral sites ($2d$) in the Li^+ jump process is energetically favored compared to direct hopping between the (electrically equivalent) octahedral sites $1b$. Squares denote vacant Li positions.

means of relaxation NMR, all Li jump processes are measured. The perfect consistency of the data points in Fig. 10 shows that ^{7}Li SAE NMR *does not* detect only a subset of the total number of Li jumps in h-$Li_{0.7}TiS_2$. Consequently, one has to conclude that the jump process probed by SAE NMR ($1b \rightarrow 2d \rightarrow 1b'$, see Fig. 11) is the only mechanism relevant in the whole temperature range covered here. Direct hopping between two octahedral sites ($1b \rightarrow 1b'$) seems to be not important for the overall cation transport. The jump distance of this process is about 3.64 Å and, thus, much larger than that for the corresponding tetrahedral-octahedral two-site process with a value of about 2.14 Å.

Quantum chemical calculations by Bredow[89] confirm these results. For $Li_{2/3}TiS_2$ an activation energy of 0.37 eV for the ($1b \rightarrow 2d \rightarrow 1b'$) pathway was calculated which is in perfect agreement with the experimental result presented here. The calculations have shown that direct hopping between two octahedral sites is energetically not favored. Quite recently, theoretical calculations by Ramírez *et al.* on Li_xTiSe_2 were performed.[39,40] Li_xTiSe_2 crystallizes in the same space group as Li_xTiS_2. Ramírez *et al.* have shown that in the isostructured Se analogue the tetrahedral-octahedral diffusion pathway is also the most probable Li migration path. Similar results were found recently by first-principles calculations for Li diffusion in Li_xCoO_2 which has a layered structure similar to that of Li_xTiS_2. Van der Ven *et al.* have shown that also in Li_xCoO_2 with $x<1$ the diffusion pathway involving tetrahedral sites is energetically favored compared to direct hopping between electrically equivalent octahedral sites.[90,91] Similar results were obtained by Catti using *ab initio* Hartree-Fock methods.[92] However, van der Ven *et al.* have found also that the latter migration path becomes more important at higher Li content x.[90] Our recent studies on a sample with $x=1.0$ indicate that this seems to be valid also for the Li_xTiS_2 system.[32,64] Interestingly, the activation energy for the tetrahedral-octahedral jump process is reduced to 0.26(1) eV for the $Li_{1.0}TiS_2$ sample. Van der Ven *et al.* have found the same trend theoretically for Li_xCoO_2.[91] Their explanation for the Li_xCoO_2 system may hold qualitatively also for the Li_xTiS_2 case: A larger electron density on the sulfur ions results in better shielding between a migrating Li^+ and the transition metal ion leading to a reduction of the activation barrier.[90,93]

Quite recently, we have demonstrated that for polycrystalline $Li_4Ti_5O_{12}$ (Ref. 67), as well as for Li_7BiO_6,[88] the activation energy obtained from ^{7}Li spin-alignment echo NMR is similar to that which is probed by dc-conductivity measurements. This similarity was also found for the interlayer Li diffusion process in single-crystalline Li_3N,[32] as well as for the cation transport in Ag ion conductors where the dynamic properties were probed by multiple-time ^{109}Ag stimulated echo NMR.[69,75] The activation energy for single-crystalline h-$Li_{\approx 0.7}TiS_2$ obtained from electrochemical methods is about 0.4 eV.[94] This value is remarkably similar to those probed by ^{7}Li SAE NMR here. Further conductivity measurements on polycrystalline h-$Li_{0.7}TiS_2$ samples are to be performed in our laboratory. Interestingly, in the present case, E_A from the low-T flanks of the NMR relaxation rate peaks agrees very well with the value from SAE NMR. This result is not self-evident. In a lot of cases significant differences between activation energies from low-T spin-lattice relaxation NMR and conductivity (as well as spin-alignment NMR) may be expected.[67,95] This difference is mainly due to the fact that both types of experiments probe ionic motion on different length and, thus, time scales. With dc-conductivity measurements, long-range diffusion parameters are probed, whereas spin-lattice relaxation NMR rates (in the laboratory frame) are sensitive to Li diffusion on a much shorter time scale (see Sec. III). Short- and long-range diffusion parameters can be considerably different, especially for structurally disordered materials with a complex potential landscape for cation migration. Additionally, the small activation energies deduced from the low-T flanks ($\omega\tau \gg 1$) of the spin-lattice relaxation rates peaks are influenced by other aspects such as strongly localized hopping of the charge carriers, or even unsuccessful attempts of the ions at jumping to a new site. These influences result in apparently low hopping barriers and higher jump rates than expected. Moreover, correlation effects due to Coloumb interactions of the moving particles will affect the slope of $T_1^{-1}(1/T)$ in the limit ($\omega\tau \gg 1$). Long-range diffusion parameters are accessible by NMR relaxation only, if the high-T flank ($\omega\tau \ll 1$) is accessible and if the structure of the material allows 3D diffusion. For a 2D ionic conductor such as Li_xTiS_2, the slope of the high-T flank is influenced by the dimensionality of the transport process (see above) and, thus, the slope of the high-T flank cannot be transformed into E_A characterizing long-range diffusion without a suitable model. Here, the nice agreement between E_A from relaxation NMR on the one hand and from SAE NMR on the other hand demonstrates that in $Li_{0.7}TiS_2$ no difference between short- and long-range diffusions exists. This results is by no means trivial. It may be expected only for a crystallographically simple structured low-defective material having a well defined as well as regular potential landscape for Li diffusion. This situation seems to be valid in the present case.

Thus, a single diffusion mechanism was probed over a large dynamic range, interestingly irrespective of the method applied. The energetically favored octahedra-tetrahedra-octahedra jump process ($1b \rightarrow 2d \rightarrow 1b'$) turned out to be the

elementary step responsible for long-range Li^+ diffusion in $Li_{0.7}TiS_2$ which is known to be two-dimensional from the NMR relaxation studies.

VII. CONCLUSION

Recording stimulated echoes for spin-3/2 spins proves to be a rather new and powerful tool for the investigation of extremely slow ionic exchange processes in crystalline ionic conductors. Here, the method was applied to the ^{7}Li nucleus. Ultraslow Li jumps were probed within the rigid lattice regime of the 2D lithium ion conductor h-$Li_{0.7}TiS_2$. In the rigid lattice range, neither the measurement of T_2^{-1} nor that of T_1^{-1} are helpful for the investigation of such slow Li jumps. Even with spin-lattice relaxation NMR measurements in the rotating frame jump rates smaller than 10^4 s^{-1} are not accessible in the present case.

However, extremely small ^{7}Li jump rates are directly obtainable via the ^{7}Li spin-alignment echo decay measured as a function of mixing time which was varied over more than six decades. In this way jump rates with values down to 0.1 s^{-1} were detectable over a dynamic range of about four decades. The corresponding correlation functions showed a two-step decay behavior. Therefore, an accurate separation of jump rates from the influence of longitudinal spin-lattice relaxation effects was possible. The data from spin-alignment echo NMR experiments fit remarkably well to those values extracted from the diffusion induced spin-lattice relaxation rate maxima recorded in the laboratory and rotating reference frame, respectively. The ^{7}Li NMR relaxation measurements as well as the ^{7}Li spin-alignment data probe one and the same diffusion process with an activation energy of about 0.4 eV. Altogether, by using this combination of NMR techniques, a solitary Li diffusion process in h-$Li_{0.7}TiS_2$ was precisely measured over a dynamic range of about ten decades. Final state amplitudes of the ^{7}Li SAE NMR two-time correlation functions reveal that octahedra-tetrahedra-octahedra jumps within the van der Waals gap between the TiS_2 layers are responsible for Li diffusion. The two-site jump process is identified as the elementary step of long-range 2D Li diffusion in h-$Li_{0.7}TiS_2$.

ACKNOWLEDGMENTS

Financial support by the Deutsche Forschungsgemeinschaft (DFG) is gratefully acknowledged. We are grateful to R. Schöllhorn and A. Payer for leaving us the sample and to W. Küchler for allowing us to include some unpublished NMR relaxation data.

*wilkening@pci.uni-hannover.de
†heitjans@pci.uni-hannover.de; www.heitjans.pci.uni-hannover.de

[1] *Lithium Ion Batteries*, edited by M. Wakihara and O. Yamamoto, (Wiley-VCH, Weinheim, 1998).
[2] J. M. Tarascon and M. Armand, Nature (London) **1414**, 359 (2001).
[3] M. S. Whittingham, Chem. Rev. (Washington, D.C.) **104**, 4271 (2004).
[4] C. Grey and N. Dupré, Chem. Rev. (Washington, D.C.) **104**, 4493 (2004).
[5] B. Scrosati, Nature (London) **373**, 557 (1995).
[6] C. Julien and G. A. Nazri, *Solid State Batteries: Materials, Design and Optimization* (Kluwer Academic, Boston, 1994).
[7] C. P. Grey and Y. J. Lee, Solid State Ionics **5**, 883 (2003).
[8] C. G. Granqvist, E. Avendaño, and A. Azens, Thin Solid Films **442**, 201 (2003).
[9] N. Imanaka, T. Kawatso, and G. Y. Adachi, Chem. Lett. **1990**, 497.
[10] C. Lee, P. K. Dutta, R. Ramamoorthy, and S. A. Akbar, J. Electrochem. Soc. **153**, H4 (2006).
[11] G. C. Farrington and J. L. Briant, Science **204**, 1371 (1979).
[12] M. S. Whittingham, Solid State Ionics **134**, 169 (2000).
[13] M. S. Whittingham, Prog. Solid State Chem. **12**, 41 (1978).
[14] M. S. Whittingham, R. Chen, T. Chirayil, and P. Zavalij, Solid State Ionics **94**, 227 (1997).
[15] R. L. Kleinberg, J. Phys. Chem. Solids **43**, 285 (1982).
[16] R. Kleinberg, B. Silbernagel, and A. Thompson, Solid State Commun. **41**, 401 (1982).
[17] R. L. Kleinberg and B. G. Silbernagel, Solid State Commun. **36**, 345 (1980).
[18] B. Silbernagel and M. Whittingham, J. Chem. Phys. **64**, 3670 (1976).
[19] K. Matsumoto, R. Nagai, T. Asai, and S. Kawai, Solid State Ionics **25**, 233 (1987).
[20] X.-P. Tang and Y. Wu, J. Magn. Reson. **133**, 155 (1998).
[21] R. Böhmer, J. Magn. Reson. **147**, 78 (2000).
[22] J. Jeener and P. Broekaert, Phys. Rev. **157**, 232 (1967).
[23] P. Heitjans, A. Schirmer, and S. Indris, in *Diffusion in Condensed Matter: Methods, Materials, Models*, 2nd ed., edited by P. Heitjans and J. Kärger (Springer, Berlin, 2005), Chap. 9, pp. 369-415.
[24] F. Fujara, S. Wefing, and H. Spiess, J. Chem. Phys. **84**, 4579 (1986).
[25] T. Dries, F. Fujara, M. Kiebel, E. Rössler, and H. Silescu, J. Chem. Phys. **88**, 2139 (1988).
[26] G. Fleischer and F. Fujara, in *NMR: Basic Principles and Progress*, edited by P. Diehl, E. Fluck, H. Günther, R. Kosfeld, and J. Seelig (Springer, Berlin, 1994), Vol. 30.
[27] M. Wilkening, W. Küchler, and P. Heitjans, Phys. Rev. Lett. **97**, 065901 (2006).
[28] R. Schöllhorn and A. Payer, Angew. Chem., Int. Ed. **24**, 67 (1985).
[29] S. Sinha and D. W. Murphy, Solid State Ionics **20**, 81 (1986).
[30] W. Küchler, P. Heitjans, A. Payer, and R. Schöllhorn, Solid State Ionics **70/71**, 434 (1994).
[31] M. Wilkening and P. Heitjans, Diffusion Fundam. **2**, 60 (2005).
[32] M. Wilkening, Ph.D. thesis, University of Hannover, 2005.
[33] M. Wilkening and P. Heitjans, Diffusion Fundam. (to be published).
[34] A. V. Powell, Annu. Rep. Prog. Chem., Sect. C: Phys. Chem. **90**, 177 (1993).
[35] A. F. McDowell, C. F. Mendelsohn, M. S. Conradi, R. C. Bowman, and A. J. Maeland, Phys. Rev. B **51**, 6336 (1995).
[36] J. Dahn, W. McKinnon, R. Haering, W. Buyers, and B. Powell,

Can. J. Phys. **58**, 207 (1980).
[37] F. Mendizábal, R. Contreras, and A. Aizman, J. Phys.: Condens. Matter **9**, 3011 (1997).
[38] W. Schattke and C. Ramírez, in *NIC Proceedings 2004*, edited by D. Wolf, G. Münster, and M. Kremer (John von Neumann Institute for Computing, Jülich, 2004), Vol. 20.
[39] C. Ramírez, R. Adelung, R. Kujz, L. Kipp, and W. Schattke, Phys. Rev. B **71**, 035426 (2005).
[40] C. Ramírez, R. Adelung, L. Kipp, and W. Schattke, Phys. Rev. B **73**, 195406 (2006).
[41] M. Meyer, P. Maass, and A. Bunde, Phys. Rev. Lett. **71**, 573 (1993).
[42] A. Bunde, W. Dieterich, P. Maass, and M. Meyer, in *Diffusion in Condensed Matter: Methods, Materials, Models*, 2nd ed., edited by P. Heitjans and J. Kärger (Springer, Berlin, 2005), Chap. 20, pp. 813–856.
[43] A. G. Redfield, Phys. Rev. **98**, 1787 (1955).
[44] D. C. Ailion and C. P. Slichter, Phys. Rev. **137**, A235 (1965).
[45] D. C. Look and I. J. Lowe, J. Chem. Phys. **44**, 2995 (1966).
[46] R. Messer and F. Noack, Appl. Phys. (Berlin) **6**, 79 (1975).
[47] P. Heitjans, A. Körblein, H. Ackermann, D. Dubbers, F. Fujara, and H.-J. Stöckmann, J. Phys. F: Met. Phys. **15**, 41 (1985).
[48] Z. Xu and J. F. Stebbins, Science **270**, 1332 (1995).
[49] V. W. J. Verhoeven, I. M. de Schepper, G. Nachtegaal, A. P. M. Kentgens, E. M. Kelder, and F. M. Mulder, Phys. Rev. Lett. **86**, 4314 (2001).
[50] J. Cabana, N. Dupré, G. Rousse, C. P. Grey, and M. R. Palacin, Solid State Ionics **176**, 2205 (2005).
[51] L. S. Cahill, R. Chapman, J. Britten, and G. Goward, J. Phys. Chem. B **110**, 7171 (2006).
[52] L. van Wüllen, N. Sofina, L. Hildebrandt, C. Mühle, and M. Jansen, Solid State Ionics **177**, 1665 (2006).
[53] L. van Wüllen, T. Echelmeyer, H.-W. Meyer, and D. Wilmer, Phys. Chem. Chem. Phys. **9**, 3298 (2007).
[54] H. W. Spiess, J. Chem. Phys. **72**, 6755 (1980).
[55] M. Lausch and H. W. Spiess, J. Magn. Reson. (1969-1992) **54**, 466 (1983).
[56] X.-P. Tang, R. Busch, W. L. Johnson, and Y. Wu, Phys. Rev. Lett. **81**, 5358 (1998).
[57] X.-P. Tang, U. Geyer, R. Busch, W. Johnson, and Y. Wu, Nature (London) **402**, 160 (1999).
[58] R. Böhmer, T. Jörg, F. Qi, and A. Titze, Chem. Phys. Lett. **316**, 419 (2000).
[59] F. Qi, T. Jörg, and R. Böhmer, Solid State Nucl. Magn. Reson. **22**, 484 (2002).
[60] F. Qi, G. Diezemann, H. Böhm, J. Lambert, and R. Böhmer, J. Magn. Reson. **169**, 225 (2004).
[61] R. Böhmer, K. Jeffrey, and M. Vogel, Prog. Nucl. Magn. Reson. Spectrosc. **50**, 87 (2007).
[62] R. Böhmer and F. Qi, Solid State Nucl. Magn. Reson. **31**, 28 (2007).
[63] F. Qi, C. Rier, R. Böhmer, W. Franke, and P. Heitjans, Phys. Rev. B **72**, 104301 (2005).
[64] M. Wilkening and P. Heitjans, Defect Diffus. Forum **237-240**, 1182 (2005).
[65] M. Wilkening, D. Gebauer, and P. Heitjans, J. Phys.: Condens. Matter **20**, 022201 (2008).
[66] M. Wilkening and P. Heitjans, J. Phys.: Condens. Matter **18**, 9849 (2006).
[67] M. Wilkening, R. Amade, W. Iwaniak, and P. Heitjans, Phys. Chem. Chem. Phys. **9**, 1239 (2006).
[68] M. Wilkening and P. Heitjans, Solid State Ionics **177**, 3031 (2006).
[69] M. Vogel, C. Brinkmann, H. Eckert, and A. Heuer, Phys. Chem. Chem. Phys. **4**, 3237 (2002).
[70] M. Vogel, C. Brinkmann, H. Eckert, and A. Heuer, J. Non-Cryst. Solids **307**, 971 (2002).
[71] M. Vogel, C. Brinkmann, H. Eckert, and A. Heuer, Solid State Nucl. Magn. Reson. **22**, 344 (2002).
[72] M. Vogel, C. Brinkmann, H. Eckert, and A. Heuer, J. Non-Cryst. Solids **352**, 5156 (2006).
[73] S. Berndt, K. R. Jeffrey, R. Küchler, and R. Böhmer, Solid State Nucl. Magn. Reson. **27**, 122 (2005).
[74] M. Vogel, C. Brinkmann, H. Eckert, and A. Heuer, Phys. Rev. B **69**, 094302 (2004).
[75] C. Brinkmann, S. Faske, M. Vogel, T. Nilges, A. Heuer, and H. Eckert, Phys. Chem. Chem. Phys. **8**, 369 (2006).
[76] A. Abragam, *The Principles of Nuclear Magnetism* (Clarendon, Oxford, 1961).
[77] W. Küchler, Ph.D. thesis, University of Hannover, 1993.
[78] W. Küchler, P. Heitjans, D. Clausen, A. Payer, and R. Schöllhorn, in *25th Congress Ampere on Magnetic Resonance and Related Phenomena*, edited by M. Mehring, J. U. von Schütz, and H. C. Wolf (Springer-Verlag, Berlin, 1990).
[79] W. Franke and P. Heitjans, Ber. Bunsenges. Phys. Chem. **96**, 1674 (1992).
[80] E. Fukushima and S. Roeder, *Experimental Pulse NMR* (Addison-Wesley, Reading, 1981).
[81] T. Springer and R. E. Lechner, in *Diffusion in Condensed Matter: Methods, Materials, Models*, 2nd ed., edited by P. Heitjans and J. Kärger (Springer, Berlin, 2005), Chap. 3, pp. 91-164.
[82] T. Bredow, P. Heitjans, and M. Wilkening, Phys. Rev. B **70**, 115111 (2004).
[83] P. M. Richards, in *Topics in Current Physics*, edited by M. B. Salamon (Springer, Berlin, 1979), Vol. 15.
[84] N. Bloembergen, E. M. Purcell, and R. V. Pound, Phys. Rev. **73**, 679 (1948).
[85] P. M. Richards, Solid State Commun. **25**, 1019 (1978).
[86] K. Funke, Prog. Solid State Chem. **22**, 111 (1993).
[87] K. L. Ngai, Comments Solid State Phys. **9**, 141 (1980).
[88] M. Wilkening, C. Mühle, M. Jansen, and P. Heitjans, J. Phys. Chem. B **111**, 8691 (2007).
[89] T. Bredow (private communication).
[90] A. van der Ven and G. Ceder, Electrochem. Solid-State Lett. **3**, 301 (2000).
[91] A. van der Ven, G. Ceder, M. Asta, and P. D. Tepesch, Phys. Rev. B **64**, 184307 (2001).
[92] M. Catti, Phys. Rev. B **61**, 1795 (2000).
[93] K. Kang and G. Ceder, Phys. Rev. B **74**, 094105 (2006).
[94] K. Kanhehori, F. Kirino, T. Kudo, and K. Miyauchi, J. Electrochem. Soc. **138**, 2216 (1991).
[95] H. Maekawa, Y. Fujimaki, H. Shen, J. Kawamura, and T. Yamamura, Solid State Ionics **177**, 2711 (2006).